Single-molecule experiment with optical tweezers: improved analysis of the diffusion of the λ-receptor in *E. coli*'s outer membrane

2003 J. Phys.: Condens. Matter 15 S1737

(http://iopscience.iop.org/0953-8984/15/18/307)

INSTITUTE OF PHYSICS PUBLISHING JOURNAL OF PHYSICS: CONDENSED MATTER

J. Phys.: Condens. Matter **15** (2003) S1737–S1746 PII: S0953-8984(03)55284-5

Single-molecule experiment with optical tweezers: improved analysis of the diffusion of the λ-receptor in *E. coli*'s outer membrane

Lene Oddershede[1], **Henrik Flyvbjerg**[2] **and Kirstine Berg-Sørensen**[1,3]

[1] Niels Bohr Institute, Blegdamsvej 17, 2100 Copenhagen, Denmark
[2] Materials Research Department, Risø National Laboratory, 4000 Roskilde, Denmark

E-mail: berg@nbi.dk

Received 28 October 2002
Published 28 April 2003
Online at stacks.iop.org/JPhysCM/15/S1737

Abstract

The motion of a single protein, a λ-receptor in the outer membrane of *E. coli*, is studied with optical tweezers. We present improved measurements and an analysis that accounts for stochastic errors, filters in the detection system, aliasing and hydrodynamic effects. We test a simple model for the protein's motion and find it in agreement with the low-frequency part of the data. We thus determine physical parameter values for the system with improved precision. The diffusion coefficient describing the motion of the λ-receptor is now obtained with 2% relative error for individual receptors, and varies between bacteria with roughly 70% root-mean-square deviation about the mean. This improved analysis also reveals that the simple model must be revised in order to agree with the high-frequency part of the power spectrum.

1. Introduction

Optical tweezers are favourite tools in the rapidly expanding field of single-molecule biophysics [1]. Recent examples of their use are studies of the motion of motor proteins such as kinesin, RNA polymerase and myosin [2–4], and of how DNA is wrapped around nucleosomes [5]. Optical tweezers are essentially non-invasive tools when the laser's wavelength is properly chosen [6]. The current resolution of reversible determination of position is as low as 3 nm [7] and forces as small as tens of femtonewtons have been measured [8]. Also, optical tweezers have been used successfully to study the motion of single proteins in membranes of living organisms, both in the eucaryotic double lipid membrane [9–13] and in the stiffer procaryotic membrane [14]. In all single-molecule investigations, precision is an issue of major concern. It is not uncommon that the first report on single-molecule measurements in a given system presents physical parameter values with large

[3] Author to whom any correspondence should be addressed.

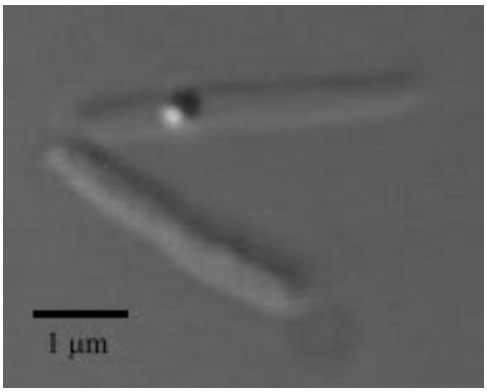

Figure 1. DIC microscopy photo showing two *E. coli* bacteria, one of them having an *in vivo* biotinylated λ-receptor in the outer membrane to which a streptavidin coated bead is attached. The diameter of the bead is 0.56 μm. A movie showing the real time motion of the receptor is also available [22].

uncertainties, sometimes larger than the values themselves [11, 12]. Precise determination of the force exerted by optical tweezers is therefore important. The maximum force that optical tweezers can exert on a dielectric bead can be measured using a flow cell [15]. The Brownian motion of a bead in a trap can be used for more precise characterizations of the trap [16–19]. For very precise measurements, however, several factors need to be accounted for [20]. These include finite sampling rate, frequency-dependent corrections to Stokes's and Faxén's hydrodynamic friction laws, the effects of electronic filters and a frequency-dependent power loss in the photo-diode detection system [20, 21].

The observation of the motion of a single λ-receptor in the outer membrane of *E. coli* was first reported in [14] using the techniques of optical tweezers and single-particle tracking based on CCD camera recordings. The λ-receptor is responsible for the transportation of maltose dextrins across the bacterial membrane. In general, receptors and porins in the bacterial membrane play an important role for transport of nutrients and drugs through the membrane.

In the experiments, a bacterium is fixed on a glass substrate and enclosed in a perfusion chamber. A streptavidin-coated polystyrene bead with a diameter of 0.56 μm is attached to a biotinylated λ-receptor, and this bead is used as a handle for the optical tweezers measurements, as illustrated in figure 1.

The construction of the *in vivo* biotinylated protein, as well as the description, preparation and controls of the bacterial system, are described in detail in [14]. Based on a simple model, physical parameters of the system were extracted: within a domain of radius $\sim$ 25 nm, the receptor was found to diffuse with a diffusion coefficient of $(1.5 \pm 1.0) \times 10^{-9}$ cm^2 s^{-1}, and the receptor was found to be confined in a harmonic potential, as if it were tethered to the bacterial cell wall by an elastic spring with spring constant of $(1.0 \pm 0.4) \times 10^{-2}$ pN nm^{-1}. The λ-receptor only moves when the bacterium has a well functioning metabolism. An example of this motion can be seen in the supplementary movie [22]. Thus, it remains unclear whether its diffusional motion is driven by thermal noise, or by a 'noise' caused by its life processes.

Here we present the results of a more careful data acquisition and analysis for the same biological system, using optical tweezers to track beads attached to the λ-receptor. Experiments were improved by acquiring longer time-series after a more careful alignment procedure. The analysis is improved by properly accounting for error bars in the power spectrum of these time-series, using analytical formulae from [20]. As a result we obtain more precise values for the physical quantities describing the system.

2. Experimental measurements

We use an optical tweezers set-up based on a $NdYVO_4$ laser with a quadrant photo-diode back focal plane detection scheme, as described in [23]. The raw data consist of time-series of voltages, V_x, V_y and V_z, created across the quadrants by light impinging on them. The voltage V_z is the sum of the voltages in all four quadrants. The other two voltages are differences: V_x is the difference between the voltages in the two quadrants to the right and the two quadrants to the left. Similarly, V_y is the difference between the top two and bottom two quadrants. From these signals we determine the position of the trapped bead, as described below. Fairly long time-series were acquired, with 2^{18} data points with sampling frequencies f_{sample} in the range 16–30 kHz, corresponding to time-series of 8.7–16.4 s duration.

In order to align the photo-diode with the laser beam, and to minimize cross-talk between the channels of the diode, a bead is trapped. The photo-diode is aligned with the laser beam by minimizing $\langle V_x \rangle$ and $\langle V_y \rangle$, both of which are calculated on-line using LabView routines. Cross-talk between the x- and y-channels of the diode is minimized by rotating the aligned diode to minimize the value of the function $P_{xy}(f)/\sqrt{P_x(f)P_y(f)}$ which is also calculated and plotted on-line [20]. Here, $P_{xy}(f) \equiv \text{Re}(\tilde{V}_x(f)\tilde{V}_y^*(f))$, and P_x and P_y are the power spectra $P_i(f) \equiv |\tilde{V}_i(f)|^2$, $i = x, y$, where $\tilde{V}_i(f)$ denotes the Fourier transformation of $V_i(t)$. For uncorrelated channels the function $P_{xy}(f)$ vanishes. If the subsequent, more precise off-line data analysis yields a non-vanishing function $P_{xy}(f)/\sqrt{P_x(f)P_y(f)}$, a simple transformation leads to uncorrelated coordinates x' and y' [20].

After this alignment procedure, the trapped bead is positioned at a location just above a bacterium. Time-series of its motion are taken in order to calibrate the trap, as described in section 3.1. The coordinates x and y of the bead, be it attached or unattached to a bacterium, are well approximated by V_x/V_z and V_y/V_z, assuming uncorrelated channels [24, 25]. Only motion in the (x, y)-plane, i.e., perpendicular to the laser beam, is analysed here.

After data have been taken for an unattached bead, this bead is allowed to escape from the trap. The sample is then moved such that a bead attached to a λ-receptor is trapped instead. By moving the sample carefully by means of a piezo-electric stage with spatial resolution of 1–2 nm, this attached bead is aligned with the laser beam and photo-detection system by minimizing $\langle V_x \rangle$ and $\langle V_y \rangle$ and by maximizing the amplitudes of V_x and V_y. The measurements reported below were performed with this alignment. With the long time-series needed for the data analysis presented here, drift of the sample during a measurement is a serious problem in the data for the bead attached to a λ-receptor. For this reason, low-frequency data are excluded from the power spectrum analysis below.

3. Theoretical models

3.1. Calibration

If a bead moving freely in solution is held in the optical trap, its movement in each spatial dimension can be modelled with a one-dimensional Langevin equation:

$$M_{\text{bead}}\ddot{x} = -\kappa x - \gamma_{\text{bead}}\dot{x} + F(t; T), \tag{1}$$

where $x(t)$ is the bead's x-coordinate at time t, M_{bead} its mass, γ_{bead} its friction with the surrounding liquid, κ the stiffness of the optical trap and $F(t; T)$ the random thermal force from the bead's surroundings resulting from the thermal motion of the liquid molecules at temperature T. The Einstein–Ornstein–Uhlenbeck theory of Brownian motion assumes this thermal force is a white noise. For the sampling rates used here, inertial forces can be neglected

and the left-hand side of equation (1) set to zero. The motion of the bead in the liquid is treated as simple Stokes flow, with friction coefficient $\gamma_{\text{bead}} = 6\pi\eta R$, for a bead of radius R moving in a liquid with dynamic viscosity η. Assuming the motion described by (1) is recorded continuously for a long time T_{meas}, we introduce its Fourier transform

$$\tilde{x}_k = \int_{-T_{\text{meas}}/2}^{T_{\text{meas}}/2} \mathrm{d}t\, \mathrm{e}^{\mathrm{i}2\pi f_k t} x(t), \qquad f_k \equiv k/T_{\text{meas}}, k \text{ integer}. \tag{2}$$

The power spectrum of the position can thus be calculated as $P(f_k) \equiv \langle|\tilde{x}_k|^2\rangle / T_{\text{meas}}$ yielding a Lorentzian [18]

$$P(f_k) = \frac{k_{\text{B}}T}{2\gamma_{\text{bead}}\pi^2(f_k^2 + f_{\text{c}}^2)} \tag{3}$$

with corner frequency $f_{\text{c}} = \kappa/(2\pi\gamma_{\text{bead}})$. As discussed in [20], experimental power spectra would be such Lorentzians if measurements were made during infinite time and with infinitely large sampling frequency. *Leakage*, the effect of a finite measurement time T_{meas}, is negligible for a smooth spectrum like a Lorentzian, while *aliasing*, the effect of finite sampling frequency, is easily taken into account [20], as done in section 4.3. Thus, with some adjustments, we use the Lorentzian (3) to fit our data.

The raw data provide time-series of the positions $x(t)$, $y(t)$ in arbitrary units. As the trapping potential is harmonic, the distributions of positions are Gaussian, characterized by a standard deviation σ in each direction that is related to the trap stiffness κ through $\sigma^2 = \frac{k_{\text{B}}T}{\kappa}$. In order to find a conversion factor from the arbitrary units to the SI unit of length, we extract the standard deviation σ in two different manners, one in units of metres, σ_{SI}, and one in arbitrary units, σ_{A}: the value of the Lorentzian at zero frequency f is $P_0 \equiv k_{\text{B}}T/(2\gamma_{\text{bead}}\pi^2 f_{\text{c}}^2) = \sigma_{\text{A}}^2/(\pi f_{\text{c}})$. Thus with f_{c} and P_0 determined from the fit, σ_{A} can be found. To determine σ_{SI}, we note that the radius of the bead, and thus also γ_{bead}, is known with only 1% error. From the fitted value of f_{c} we find κ and thereby extract a value for σ_{SI}. The ratio between σ_{SI} and σ_{A} provides the desired conversion factor. This procedure is different from the one outlined in [14] where the value of σ_{A} was determined from the position histogram. As the position histogram is broadened by low-frequency noise (drift) and narrowed by low-pass filters in the data acquisition pathway, the method presented here provides more precise values because these causes of systematic errors can be detected and circumvented. We used this calibration procedure with all samples and laser intensities.

3.2. Bead attached to protein

We monitor the position of the bead in time, but really want to study the protein it is attached to. In order to extract the dynamics of the protein's position in the outer membrane from the measured positions of the bead, a model introduced in [14] is used. It is assumed that the noise driving the motion of the protein is thermal, an issue subject to further investigations. The attachment between the streptavidin coated bead and the biotinylated λ-receptor is modelled as harmonic, with κ_{bs} denoting the spring constant of the biotin–streptavidin binding. The protein is assumed to be harmonically attached to something inside the cell, putatively the bacterial cell wall. This assumption is supported by experimental evidence [14] and we denote the spring constant of this harmonic tether κ_{cw}. The last new parameter in the model is γ_{prot}, the friction coefficient describing the frictional force from the bacterial outer membrane on the moving protein.

With the reasonable assumption (see arguments in [14]) that $\kappa_{\rm bs} \gg \kappa, \kappa_{\rm cw}$ and in the relevant frequency range ($f \ll \frac{\kappa_{\rm bs}}{2\pi\gamma_{\rm prot}} \simeq 10^7$ Hz) the power spectrum reduces to

$$P_{\rm bead}(f) \simeq \frac{k_{\rm B}T}{2\pi^2(\gamma_{\rm prot}+\gamma_{\rm bead})(f^2+{f_{\rm c,\lambda}}^2)} \tag{4}$$

with corner frequency

$$f_{\rm c,\lambda} = \frac{\kappa+\kappa_{\rm cw}}{2\pi(\gamma_{\rm prot}+\gamma_{\rm bead})}. \tag{5}$$

Hence, the protein–bead complex has a power spectrum as if it were a single object moving in a liquid with a friction coefficient $\gamma_{\rm prot}+\gamma_{\rm bead}$, held in a harmonic potential of spring constant $\kappa_{\rm cw}+\kappa$, and with a corner frequency equal to $f_{\rm c,\lambda}$.

The power spectrum of the position of the attached bead, (4), contains two unknowns, $\kappa_{\rm cw}$ and $\gamma_{\rm prot}$, which both are determined from the fitted parameters $P_{0,\lambda}$ and $f_{\rm c,\lambda}$. A diffusion coefficient for the protein, $\mathcal{D}_{\rm prot}$, is extracted via the Einstein relation, $\mathcal{D}_{\rm prot} = k_B T/\gamma_{\rm prot}$.

There is no experimental evidence for anisotropy in the physical parameters with respect to any bacterial coordinate system. Therefore, the values $\kappa_{\rm cw}$, $\gamma_{\rm prot}$ and diffusion coefficient $\mathcal{D}_{\rm prot}$ are defined and calculated independently of choice of coordinate system, as discussed in [14].

4. Data analysis

4.1. Blocking

In the following power spectral analysis, it is important that the experimentally obtained power spectral values $P^{(\rm ex)}(f)$ are uncorrelated for different values of f. To this end, the entire time-series is fast Fourier transformed without using data windowing [26]. Instead, the number of data points and their noise are reduced by blocking: a 'block' of n consecutive data points, $(f, P^{(\rm ex)}(f))$, of the experimental power spectrum $P^{(\rm ex)}(f)$ is replaced with one point $(\bar{f}, \bar{P}^{(\rm ex)}(\bar{f}))$, where

$$\bar{f} = \frac{1}{n_{\rm block}} \sum_{f\in{\rm block}} f; \qquad \bar{P}^{(\rm ex)} = \frac{1}{n_{\rm block}} \sum_{f\in{\rm block}} P^{(\rm ex)}(f). \tag{6}$$

As shown in [20], the data points of the raw experimental power spectrum are exponentially distributed. But with sufficiently large $n_{\rm block}$, the central limit theorem ensures that the blocked data points are Gaussian distributed, and standard least-squares fitting of the theoretical spectrum P to the blocked data points can be done. The theoretical spectrum represents the expectation value for experimental power spectral values. The scatter of the latter about their mean is known as well,

$$\langle \bar{P}^{(\rm ex)}(\bar{f})\rangle = P(\bar{f}) \tag{7}$$

$$\sigma(\bar{P}^{(\rm ex)}(\bar{f})) = \sigma(P^{(\rm ex)}(\bar{f}))/\sqrt{n_{\rm block}} = P(\bar{f})/\sqrt{n_{\rm block}}. \tag{8}$$

Blocking can be done either on a logarithmic or linear frequency axis. As long as the theoretical power spectrum is well approximated by a straight line within each block, either method is equally good. Blocking on a linear axis is more easily implemented in a program, while blocking on a logarithmic axis is more suitable for graphical presentation in a double-log plot of the spectrum.

4.2. Simple Lorentzian fit

Equations (3) and (4) suggest fitting the data by simple Lorentzians if sampling is done with an infinite sampling rate. When sampling rates and times are not infinite, the Lorentzian form can still be a reasonable model for the power spectrum at frequencies small compared to the Nyquist frequency and small compared to the diode's unintended filter frequency [20]. For our set-up this restricts our frequency range to $f < f_{\max} \sim$ 1–2 kHz. The result of a least-squares fit of the Lorentzian is known analytically. It is given as closed formulae for the fitting parameters f_c and P_0 (or $f_{c,\lambda}$ and $P_{0,\lambda}$) as functions of the experimental spectrum [20],

$$f_c = \left(\frac{S_{0,1} S_{2,2} - S_{1,1} S_{1,2}}{S_{1,1} S_{0,2} - S_{0,1} S_{1,2}} \right)^{\frac{1}{2}} \tag{9}$$

$$P_0 f_c^2 T_{\text{meas}} = \frac{S_{0,2} S_{2,2} - S_{1,2}^2}{S_{1,1} S_{0,2} - S_{0,1} S_{1,2}} \tag{10}$$

where $S_{p,q}$ are sums over experimental data,

$$S_{p,q} \equiv \sum_{k=1}^{N'} f_k^{2p} \bar{P}_k^{(\text{ex})q} \tag{11}$$

and f_k are the discrete frequencies at which the experimental power spectral values are given. The maximum index N' corresponds to $f_{\max}$: $f_{N'} = f_{\max}$, and it is assumed that $f_{N'}$ is somewhat larger than f_c. Analytical formulae for the standard deviations of f_c and P_0, as well as for the covariance between these fitting parameters, are also known [20].

4.3. Filtered and aliased power spectrum

In order to improve precision, it is desirable to use all available data and fit up to $f_{\max} = f_{\text{Nyq}} \equiv f_{\text{sample}}/2$. In order to do this, we need to take several factors into account [20]: hydrodynamic corrections, the effect of aliasing due to the finite sampling frequency, the effect of electronic filters and the unintended filtering done by the photo-detection system [21]. To our knowledge, no existing theory describes hydrodynamic corrections to Stokes's and Faxén's laws in a manner useful for the system studied here. The reason for this is that the hydrodynamic environment is very complex as the beads are close to the rough bacterial surface and the bacteria themselves are attached to the cover-slip such that the distance between the centre of the bead and the cover-slip is approximately 1–2 μm. As a first approximation, we anticipate that the effects of frequency-dependent hydrodynamic corrections are small. This is demonstrated to hold far from surfaces by the dashed curve in [20, figure 5] for the small bead-size we use here. Also, as the motion of the protein–bead complex is dominated by the motion of the protein, minor corrections to the motion of the bead would have little influence on the motion of the protein.

It is, however, important to include the effect of electronic filters and, in particular, the filtering effect of the photo-detection system [20, 21]. They are all first-order filters, each with its own roll-off frequency, $f_{3\text{dB}}$. Also, we include the effect of aliasing caused by finite sampling frequency. Altogether this results in the following expression, to be fitted to the experimental data:

$$P_{\text{F\&A}}(f) = \sum_{n=-\infty}^{n=\infty} P_{\text{Lorentz}}(f + 2n f_{\text{Nyq}}) F_{\text{elec}}(f + 2n f_{\text{Nyq}}) F_{\text{diode}}(f + 2n f_{\text{Nyq}}) \tag{12}$$

where $P_{\text{Lorentz}}(f)$ is the Lorentzian power spectrum. In the case of an unattached bead in a trap, $P_{\text{Lorentz}}(f)$ is given by (3). In the case of a bead attached to a protein $P_{\text{Lorentz}}(f)$ is given by (4). In both cases, $P_{\text{Lorentz}}(f)$ contains two parameters which are determined by fitting.

The effects of the filters are described by their characteristics, $F_{\rm elec}(f)$ and $F_{\rm diode}(f)$ for the electronic and the diode filters, respectively. They are given by

$$F_{\rm elec}(f) = \prod_j \frac{1}{1 + (f/f_{\rm 3dB}^{(j)})^2} \tag{13}$$

and

$$F_{\rm diode}(f) = \frac{1}{1 + (f/f_{\rm 3dB}^{(\rm diode)})^2} \tag{14}$$

where the product over j is over all electronic filters in the acquisition pathway. Equation (14) is valid for the data used here for which $f_{\rm Nyq} \leqslant f_{\rm 3dB}^{(\rm diode)}$. The values of $f_{\rm 3dB}^{(j)}$ for our electronic filters are known: one is fixed at 80 kHz, the other is set to either 20 or 50 kHz. As $f_{\rm 3dB}^{(\rm diode)}$ depends on the laser intensity, it enters as a third fitting parameter [20, 21] in the fits to the power spectrum of the unattached bead. In practice, the sum in (12) is performed for n in the range $n \in [-100, 100]$.

5. Results

Figure 2 shows the power spectrum of the position of a bead in solution, trapped by the optical tweezers (squares), and of a bead attached to a protein in the bacterial outer membrane, and also held with the optical tweezers (circles). The data have been blocked on the logarithmic frequency axis in order to allow the eye to distinguish individual data points. Each data point carries error bars of one standard deviation. These error bars decrease exponentially with frequency and are invisible at higher frequencies.

Figure 2 also shows fits of Lorentzians and the filtered and aliased theoretical power spectrum to the data: the full lines are Lorentzian fits, obtained using (9) and (10) with data between $f_{\rm min} = 80$ Hz and $f_{\rm max} = 1$ kHz. This value for $f_{\rm min}$ was chosen to avoid effects of low-frequency noise, caused mainly by mechanical drift. As discussed in [20], precision on both P_0 and $f_{\rm c}$ is possible even with $f_{\rm min}$ close to $f_{\rm c}$ since the entire frequency range carries information about both of these fitting parameters. A change in P_0, e.g., corresponds to a translation of the entire power spectrum along the y-axis, so only high-frequency data are needed to determine P_0.

The supports, or goodnesses of fit [26, 27] of the two Lorentzian fits are 35% for the fit to the power spectrum of the attached bead, and 25% for the unattached one. For the bead attached to a λ-receptor, the values obtained for the fitting parameters are $f_{\rm c,\lambda} = 90 \pm 4$ Hz and $P_{0,\lambda} = 68 \pm 4$ (arb. units)^2 s^{-1}. For the unattached bead, the values are $f_{\rm c} = 93 \pm 3$ Hz and $P_0 = (5.3 \pm 0.3) \times 10^2$ (arb. units)^2 s^{-1}.

The results of fitting the filtered and aliased theoretical power spectrum, (12), to data between $f_{\rm min} = 80$ Hz and $f_{\rm max} = f_{\rm Nyq}$ are shown as dashed curves. For the unattached bead, the goodness of the fit is 19% [26, 27]. In this fit the fitting parameters are $f_{\rm c} = 91 \pm 3$ Hz and $P_0 = (5.5 \pm 0.4) \times 10^2$ (arb. units)^2 s^{-1}, in agreement with the Lorentzian fit. The inset shows the quality of this fit to the filtered and aliased theoretical power spectrum; it is almost perfect, as indicated already by its support. The 3 dB frequency of the diode, $f_{\rm 3dB}^{(\rm diode)}$, was found to be 13.1 ± 0.1 kHz. This is slightly higher than in previous studies with the same set-up [20, 21], but reasonable as it depends on the laser intensity. Unknown systematic errors, e.g., of hydrodynamic origin, may affect this value. With the precision of the procedure used here, however, no acceptable fit of the filtered and aliased theoretical power spectrum to the data for a bead attached to a λ-receptor could be obtained. The χ^2-value per degree of freedom was larger than ten for all such spectra. In the concluding section, we shall return to

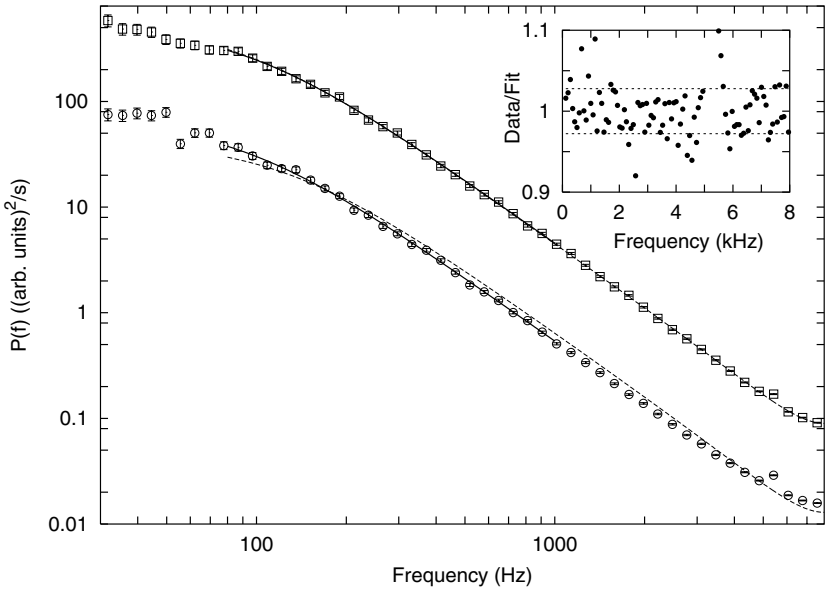

Figure 2. Power spectra of the positions of two beads in optical traps. Circles: power spectrum of bead attached to λ-receptor in bacterial outer membrane. Squares: power spectrum of bead in solution. The full lines are Lorentzian fits to data between 80 and 1 kHz, done using equations (9)–(10). Dashed lines are fits to data above $f_{\min} = 80$ Hz, using the filtered and aliased theoretical power spectrum (12), with exclusion of the data point at 5.5 kHz which is contaminated by electronic noise. The inset shows residual values, i.e., blocked data, divided by fitted value, for the fit of (12) to the spectrum for the bead in solution. Horizontal dashed lines represent ±1 standard deviation for the residues.

this point. In the following, the parameters resulting from the Lorentzian fits in the frequency range [80, 1000 Hz] are used to describe the physical properties of the λ-receptor system.

We calculated γ_{prot} and κ_{cw} from the fitted value of $f_{\text{c},\lambda}$ and $P_{0,\lambda}$, the known value for γ_{bead}, and the value for κ obtained in the calibration of the trap with an unattached bead. Figure 3(a) shows the value of γ_{prot}, and figure 3(b) the value of κ_{cw} as a function of applied laser intensity. In the data acquisition, only laser intensities below the opticution threshold determined in [14] were applied. Different samples are distinguished by different symbols. Results of six measurements with bacteria from two independent cultures are shown. Only samples that gave consistent Lorentzian fits, i.e., fits with a goodness of fit larger than 5% [26, 27], were included. For a comparison with data acquired and analysed in a simpler fashion, the values for γ_{prot} and κ_{cw} of [14] for the same system are shown in the two insets of figure 3. Note the larger range on the intensity axes of the inset.

Figure 3 maybe indicates that the data analysis used here resolves differences in physical characteristics between different receptors (on different bacteria): two measurements on the same receptor, but with different trap strengths, give identical values for physical characteristics within error bars (in two out of three cases), while measurements on different receptors give significantly different values. In other words, we seem to have reduced the experimental error bar on our analysis to a level so low that variations in the biological system itself are responsible for the largest scatter in results.

Under the assumption that we *are* able to resolve the characteristics of different receptors, we have three independent measurements of the quantities we are after, each

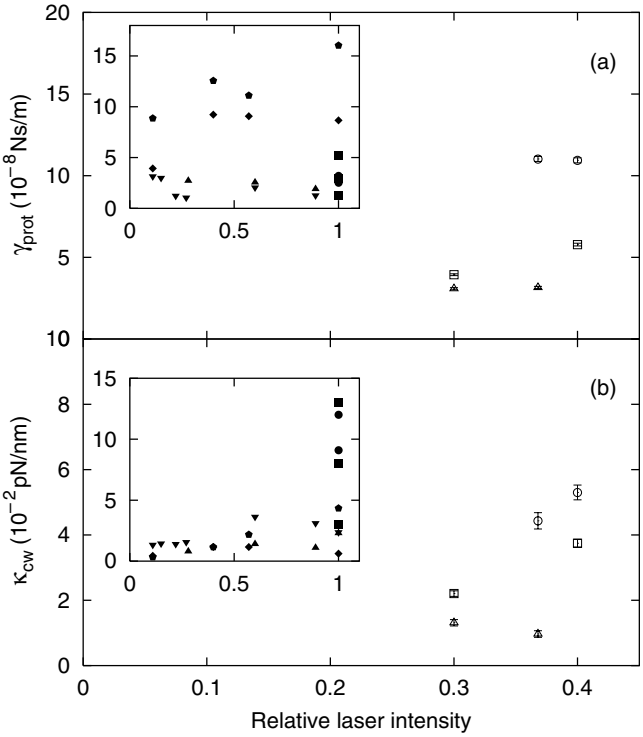

Figure 3. Physical parameters characterizing the motion of a single λ-receptor in the bacterial outer membrane. The parameters were obtained from fits to the low-frequency part of the power spectrum. The insets show data published in [14]. Independent samples are distinguished by different symbols. With the improved precision we seem to resolve differences between individual bacteria. (a) Friction coefficient γ_{prot} describing the friction exerted by the bacterial outer membrane on the diffusing λ-receptor. (b) Spring constant κ_{cw} characterizing the harmonic force between protein and bacterium, possibly a tether attached to the bacterial cell wall.

drawn from the same unknown distribution. Our three measurements for γ_{prot} give as best estimates for the mean and root-mean-square deviation (RMSD) of this distribution $\bar{\gamma}_{prot} = (6 \pm 2) \times 10^{-8}$ Ns m^{-1} and $\sigma_{\gamma_{prot}} = (4 \pm 2) \times 10^{-8}$ Ns m^{-1}. Consequently, $\mathcal{D}_{prot}$ for different receptors is distributed with mean $\bar{\mathcal{D}}_{prot} = (6.5 \pm 2.6) \times 10^{-10}$ cm^2 s^{-1} and RMSD $\sigma_{\mathcal{D}_{prot}} = (4.4 \pm 2.2) \times 10^{-10}$ cm^2 s^{-1}. The value $\bar{\mathcal{D}}_{prot} = (15 \pm 10) \times 10^{-10}$ cm^2 s^{-1} reported in [14] is consistent with this result. The spring constant describing the connection between protein and bacterial cell wall is distributed with mean $\bar{\kappa}_{cw} = (3 \pm 1) \times 10^{-2}$ pN nm^{-1} and RMSD $\sigma_{\kappa_{cw}} = (2 \pm 1) \times 10^{-2}$ pN nm^{-1}. This value for $\bar{\kappa}_{cw}$ is somewhat larger than our earlier result $(1.0 \pm 0.4) \times 10^{-2}$ pN nm^{-1} [14].

6. Conclusion

We have applied the improved data acquisition and analysis for optical tweezers of [20] to the biophysical single-molecule experiment of [14], describing the motion of a single λ-receptor in the bacterial outer membrane.

Using data at low frequencies, precise estimates for the physical parameters of the biological system were obtained. Diffusion coefficients and spring constants for individual bacteria were determined with a relative uncertainty as low as 2%, so we are maybe able

to resolve differences between individual receptors/bacteria, though more experiments are needed before we can conclude this firmly. The precision achieved here is highly relevant for measurements of changes in the motion of the λ-receptor, e.g., in response to chemical attacks on the bacterial cell wall.

Furthermore, the power spectrum of the free bead was fitted to perfection in its entire frequency range with a functional form that includes most of the effects described in [20]: electronic filters, frequency-dependent response of our photo-detection system and aliasing due to finite sampling rate. Yet, the same functional form would not fit the attached bead's power spectrum. This failure was not due to noise in the data. Thus, we seem to have reached a level of precision that requires a refined treatment of our model at higher frequencies, an issue we intend to address in the near future.

References

[1] Special issue on single molecule biophysics 1999 *Science* **March** 12
[2] Wang M, Schnitzer M, Yin H, Landick R, Gelles J and Block S 1998 *Science* **282** 902
[3] Veigel C, Bartoo M, Sellers J and Molloy J E 2002 *Nature Cell Biol.* **4** 59
[4] Schnitzer M J, Visscher K and Block S M 2000 *Nature Cell Biol.* **2** 718
[5] Brower-Toland B, Smith C, Yeh R, Lis J, Peterson C and Wang M 2002 *Proc. Natl Acad. Sci. USA* **99** 1960
[6] Neuman K C, Chadd E H, Liou G F, Bergman K and Block S M 1999 *Biophys. J.* **77** 2856
[7] Lang M, Asbury C, Shaevitz J and Block S 2002 *Biophys. J.* **83** 491
[8] Meiners J C and Quake S R 2000 *Phys. Rev. Lett.* **84** 5014
[9] Pralle A, Keller P, Florin E L, Simons K and Hörber J K H 2000 *J. Cell Biol.* **148** 997
[10] Suzuki K, Sterba R E and Sheetz M P 2000 *Biophys. J.* **79** 448
[11] Kusumi A, Sako Y and Yamamoto M 1993 *Biophys. J.* **85** 2021
[12] Sako Y and Kusumi A 1994 *J. Cell Biol.* **125** 1251
[13] Sako Y and Kusumi A 1995 *J. Cell Biol.* **129** 1559
[14] Oddershede L, Dreyer J K, Grego S, Brown S and Berg-Sørensen K 2002 *Biophys. J.* **83** 3152–61
[15] Svoboda K and Block S 1994 *Annu. Rev. Biophys. Biomol. Struct.* **23** 247
[16] Simmons R M, Finer J T, Chu S and Spudich J A 1996 *Biophys. J.* **70** 1813
[17] Visscher K and Block S M 1998 *Methods Enzymol.* **298** 460
[18] Gittes F and Schmidt C F 1998 *Methods Cell Biol.* **55** 129
[19] Florin E L, Pralle A, Stelzer E H K and Hörber J K H 1998 *Appl. Phys.* A **66** S75
[20] Berg-Sørensen K and Flyvbjerg H 2003 *Biophys. J.* submitted
[21] Berg-Sørensen K, Oddershede L, Florin E L and Flyvbjerg H 2002 *J. Appl. Phys.* at press
[22] Movie showing the motion of a single λ-receptor in the bacterial outer membrane in real time www.iop.org/EJ/journal/JPhysCM
[23] Oddershede L, Grego S, Nørrelykke S F and Berg-Sørensen K 2001 *Probe Microsc.* **2** 129
[24] Gittes F and Schmidt C F 1998 *Opt. Lett.* **23** 7
[25] Pralle A, Prummer M, Florin E L, Stelzer E H K and Hörber J K H 1999 *Microsc. Res. Techn.* **44** 378
[26] Press W H, Flannery B P, Teukolsky S A and Vetterling W T 1986 *Numerical Recipes* (Cambridge: Cambridge University Press)
[27] Barford N C 1986 *Experimental Measurements: Precision, Error and Truth* 2nd edn (New York: Wiley)